

Shear-induced self-diffusion and microstructure in non-Brownian suspensions at non-zero Reynolds numbers

By JANNEKE KROMKAMP^{1,2}, DIRK T. M. VAN DEN ENDE³,
DRONA KANDHAI⁴, RUUD G. M. VAN DER SMAN¹
AND REMKO M. BOOM¹

¹Food and Bioprocess Engineering Group, Wageningen University, Wageningen, The Netherlands

²Corporate Research, Friesland Foods BV, Deventer, The Netherlands

³Science and Technology, University of Twente, Enschede, The Netherlands

⁴Kramers Laboratorium voor Fysische Technologie, Delft University of Technology, Delft,
The Netherlands

(Received 30 June 2003 and in revised form 15 October 2004)

This paper addresses shear-induced self-diffusion in a monodisperse suspension of non-Brownian particles in Couette flow by two-dimensional computer simulations following the lattice-Boltzmann method. This method is suited for the study of (many-particle) particulate suspensions and can not only be applied for Stokes flow, but also for flow with finite Reynolds number. At relatively low shear particle Reynolds numbers (up to 0.023), shear-induced diffusivity exhibited a linear dependence on the shear rate, as expected from theoretical considerations. Simulations at shear particle Reynolds numbers between 0.023 and 0.35, however, revealed that in this regime, shear-induced diffusivity did not show this linear dependence anymore. Instead, the diffusivity was found to increase more than linearly with the shear rate, an effect that was most pronounced at lower area fractions of 0.10 and 0.25. In the same shear regime, major changes were found in the flow trajectories of two interacting particles in shear flow (longer and closer approach) and in the viscosity of the suspension (shear thickening). Moreover, the suspended particles exhibited particle clustering. The increase of shear-induced diffusivity is shown to be directly correlated with this particle clustering. As for shear-induced diffusivity, the effect of increasing shear rates on particle clustering was the most intensive at low area fractions of 0.10 and 0.25, where the radius of the clusters increased from about 4 to about 7 particle radii with an increase of the shear Reynolds number from 0.023 to 0.35. The importance of particle clustering to shear-induced diffusion might also indicate the importance of other factors that can induce particle clustering, such as, for example, colloidal instability.

1. Introduction

In concentrated non-Brownian suspensions, shear-induced diffusion affects the motion of the suspended particles and is consequently of major importance for the flow behaviour of these suspensions. A variety of interesting rheological phenomena in concentrated suspensions is invoked by shear-induced diffusion, such as viscous resuspension (during sedimentation and cross-flow filtration) and particle segregation

in radial and pipe flow (see e.g. Chapman & Leighton 1991; Lyon & Leal 1998). Therefore, this subject has attracted considerable attention from researchers, starting with the first direct experimental study of Eckstein, Bailey & Shapiro in 1977. Later, theoretical as well as numerical work followed (see e.g. Brady & Morris 1997; Drazer *et al.* 2002).

In contrast to the more familiar diffusion concepts of Brownian diffusion and turbulent diffusion, which are, respectively, caused by thermal fluctuations and inertial effects, shear-induced diffusion is caused by hydrodynamic particle–particle interactions. The diffusivity of the particles is the result of the spatial hindrance that they experience in a concentrated suspension which is macroscopically forced to flow. Although this process in principle is a deterministic process, it can be described as a diffusion process owing to the complex nature of the hydrodynamics.

A distinction can be made between shear-induced self-diffusion and shear-induced gradient diffusion (or migration). The first concept considers the motion of individual particles in a homogeneous suspension, whereas the latter considers collective particle migration in the presence of a gradient. This paper addresses the concept of shear-induced self-diffusion only.

To obtain information about shear-induced self-diffusion, the motion of individual particles in a suspension must be monitored. Experimental work is mostly carried out with the use of tracer particles in a suspension. An overview of experimental data on shear-induced self-diffusion is given by Breedveld *et al.* (1998, 2001). Unfortunately, experimental techniques mostly impose severe limitations on the range of strain values during which the particles can be monitored, which complicates the work on shear-induced self-diffusion considerably. Theoretical analyses and numerical computations can therefore be helpful for comparison and for information that cannot be obtained with experiments.

A theoretical approach of shear-induced self-diffusion is complicated by the fact that a two-body system in the presence of only hydrodynamic interactions, either does not exhibit diffusive behaviour (for the motion parallel to the velocity gradient and vorticity directions) or exhibits singular behaviour (for the motion parallel to the fluid velocity). Approaches that have been applied to overcome this problem in the theoretical computation of shear-induced diffusion, are the introduction of an additional pair of particles (Acrivos *et al.* 1992), examination of three particle interactions (Wang, Mauri & Acrivos 1996), introduction of surface roughness on the particles (Da Cunha & Hinch 1996) and introduction of residual Brownian motion and a hard-sphere interparticle force (Brady & Morris 1997). The latter approach by Brady & Morris can be considered the most successful up to now. It predicts the correct level of anisotropy between the diffusion in the velocity gradient (D_{yy}) and vorticity (D_{zz}) direction. The calculated diffusivities are, however, a factor of about six higher than values from experimental studies. Moreover, the theory predicts a continuous increase of the diffusion coefficient with volume fraction, while experimental values level off at high volume fractions. We can therefore conclude that, in spite of the aforementioned rigorous attempts, up to now, no theory is available that satisfactorily predicts shear-induced diffusive behaviour.

Some numerical studies on shear-induced diffusion have been reported using Stokesian dynamics (SD) simulations (Yurkovetsky 1998; Foss & Brady 1999; Marchioro & Acrivos 2001; Drazer *et al.* 2002). Many-body hydrodynamic interactions are included in this simulation technique. The SD simulations provided self-diffusion coefficients that are of the same order of magnitude as experimental results. The computed anisotropy between D_{yy} and D_{zz} also compared well with experimental

data. Although the SD simulations strongly contributed to the level of understanding of shear-induced diffusion, the results of the simulations are not uncontroversial. The dependence of the diffusion coefficient on the volume fraction, for example, is not clear. While earlier work shows a continuous growth of the diffusion coefficient with the volume fraction, recent work suggests the existence of a plateau at high volume fractions (Foss & Brady 1999; Marchioro & Acrivos 2001). This plateau was, however, only found for D_{yy} and not for D_{zz} . Another controversial aspect is the number of particles incorporated in the system. The computational costs for calculations on non-colloidal systems (dominated by hydrodynamics) are very high with SD and in most published work, systems were used with 27 particles only. Since this system size is small compared to any realistic system, the results have to be treated with caution. The recent introduction of the accelerated Stokesian dynamics (ASD) simulation technique (Sierou & Brady 2001), based on a much faster computational algorithm, allows the study of large systems with typically 1000 suspension particles. Using ASD to study shear-induced self-diffusion, Sierou & Brady (2004) indeed showed the relevance of high particle numbers and sufficiently high strains for reliable diffusion coefficients. Their results, covering the full diffusivity tensor, can probably be considered the most accurate up to now.

Besides the relatively high computational cost, SD, and also ASD, have other limitations for the simulation of shear-induced diffusion. The suspending fluid is assumed to be Newtonian and to be flowing under conditions approximating Stokes flow (particle Reynolds number $Re_p \rightarrow 0$). Although ASD may have better possibilities, with SD, the application of non-spherical particle shapes and size distributions is complex. Moreover, it is difficult to make the method suitable for simulations in bounded regimes with container walls (Ladd & Verberg 2001). These aspects may be of importance to gain a better insight into shear-induced diffusion in practical systems. Therefore, although SD and ASD are robust methods that accurately resolve hydrodynamic interactions, they are not yet able to address all relevant aspects of shear-induced diffusion.

In this paper, a study on shear-induced diffusion is presented making use of a lattice-Boltzmann (LB) model for particulate suspensions (Ladd & Verberg 2001). This model combines Newtonian dynamics of solid particles with a discretized Boltzmann equation for the fluid phase. The many-body hydrodynamic interactions are fully accounted for (with inclusion of an explicit lubrication force for hydrodynamic interactions over very short distances). However, the LB model may have a number of advantages for the simulation of shear-induced diffusion over the SD model. Since the interactions between the fluid and the suspended solid particles can be calculated with simple local rules, the computational cost depends linearly on the amount of suspended particles, which makes many-particle simulations feasible. The LB model is also not restricted to the Stokes flow regime for fluid flow and can easily be applied for non-spherical particles, for particles with a size distribution and for systems bounded by container walls (Ladd & Verberg 2001). This may make the LB technique more suitable for the simulation of shear-induced diffusion in more complex systems, where the aforementioned aspects play a role.

The aim of this work is to examine shear-induced diffusion outside the Stokes flow regime, at finite Reynolds numbers, and investigate the effect of inertia. The fact that these conditions of finite Reynolds numbers are frequently applied in (industrial) processes of suspensions, such as milk and other foods, paints and river water, makes the relevance of this work evident. Although it is well-known that the rheological behaviour of concentrated suspensions can become non-Newtonian in this regime, as

far as we know, the scaling of shear-induced diffusion with the shear rate has not been studied yet. In this study, we furthermore compare the shear-induced diffusive behaviour with the effects of shear on the flow trajectories of one particle and two interacting particles and on the viscosity of a multi-particle suspension, so as to be able to detect possible correlations. The study is carried out for two-dimensional systems in order to limit the computational costs. Although this might lead to differences in the scaling of the relations in comparison with three-dimensional systems, the trends will be similar.

In §2, we present an outline of our LB method for particulate suspensions. Subsequently, we show results of the shear-dependent behaviour of one (flow trajectory), two (flow trajectory) and multi-particle (viscosity) systems. In §4, we present our results on shear-induced diffusion. As a relevant parameter, in §5, an analysis is made of the suspension microstructure at different shear rates, whereafter we draw our conclusions.

2. Computer simulation method

We have applied the LB method in our simulations. Since this method has already been outlined extensively in literature (see e.g. Ladd 1994a; Ladd & Verberg 2001), we will only recapitulate the most important points. The LB method models a compressible fluid (in which the speed of sound is finite) in the limit of low Mach number ($Ma = \text{flow velocity}/\text{speed of sound}$), by solving the discretized Boltzmann equation for fictitious fluid particles, that are constrained to move on a lattice. The state of the fluid is characterized by the single-particle distribution function $f_i(\mathbf{x}, t)$, describing the average number of particles at a particular node of the lattice \mathbf{x} , at a time t , with the discrete velocity \mathbf{c}_i , which brings the fluid particles in one time step to an adjacent lattice node. In the simulations described in this paper, the fluid dynamics were solved with a D2Q9 LB scheme, which is defined on a two-dimensional square lattice with rest particles and 8 non-zero particle velocities. The velocity directions link lattice sites to its nearest and next-nearest neighbours. The velocity vectors on this two-dimensional lattice are defined as:

$$\mathbf{c}_i = \begin{cases} (0, 0), & i = 0, \\ (\cos \frac{1}{2}(i-1)\pi, \sin \frac{1}{2}(i-1)\pi), & i = 1, 2, 3, 4, \\ \sqrt{2}(\cos(\frac{1}{2}(i-1)\pi + \frac{1}{4}\pi), \sin(\frac{1}{2}(i-1)\pi + \frac{1}{4}\pi)), & i = 5, 6, 7, 8. \end{cases} \quad (2.1)$$

The hydrodynamic fields mass density ρ , momentum density \mathbf{j} , and the momentum flux density $\mathbf{\Pi}$ are moments of this velocity distribution:

$$\rho = \sum_i f_i, \quad \mathbf{j} = \sum_i f_i \mathbf{c}_i, \quad \mathbf{\Pi} = \sum_i f_i \mathbf{c}_i \mathbf{c}_i. \quad (2.2)$$

The fictitious fluid particles evolve by collisions and subsequent propagation to neighbouring lattice sites. This two-step process is described by the following equations:

$$f'_i(\mathbf{x}, t) = f_i(\mathbf{x}, t) - \sum_j \mathbf{\Omega}_{ij} f_j^{neq}(\mathbf{x}, t), \quad (2.3)$$

$$f_i(\mathbf{x} + \Delta \mathbf{x}_i, t + \Delta t) = f'_i(\mathbf{x}, t). \quad (2.4)$$

Here, $f'_i(\mathbf{x}, t)$ is the post-collisional distribution function. The non-equilibrium part of the distribution function is defined as $f_i^{neq}(\mathbf{x}, t) = f_i(\mathbf{x}, t) - f_i^{eq}(\mathbf{x}, t)$. The lattice

spacing is defined as $\Delta \mathbf{x}_i = \mathbf{c}_i \Delta t$. The collision operator Ω_{ij} controls the shear stress relaxation at every lattice site. In our simulations, we applied the collision operator of the BGK model (Bhatnagar, Gross & Krook 1954; Qian, d'Humières & Lallemand 1992), which is a simplification of the full LB model. The BGK collision operator is defined such that the distribution functions are simply relaxed at each time step towards the local equilibrium distribution with the relaxation time τ :

$$f_i(\mathbf{x} + \Delta \mathbf{x}_i, t + \Delta t) = f_i(\mathbf{x}, t) - \frac{f_i(\mathbf{x}, t) - f_i^{eq}(\mathbf{x}, t)}{\tau}. \quad (2.5)$$

The relaxation time τ controls the relaxation of the viscous stress in the fluid and is linked to the kinematic viscosity ν via:

$$\nu = c_s^2 \left(\tau - \frac{1}{2} \right) \Delta t, \quad (2.6)$$

where the speed of sound c_s is defined by $c_s^2 = c^2/3$. In our simulations, we applied $\tau = 1.0$ (in lattice units), which corresponds to a kinematic viscosity ν of the fluid of $1/6$ (in lattice units). The equilibrium distribution $f_i^{eq}(\mathbf{x}, t)$ is chosen such that the Navier–Stokes equations for a weakly compressible system are obtained (Frisch, Hasslacher & Pomeau 1986). It can be expressed as a series expansion in powers of the flow velocity \mathbf{u} :

$$f_i^{eq} = \rho w_i \left(1 + \frac{1}{c_s^2} \mathbf{u} \cdot \mathbf{c}_i + \frac{1}{2c_s^4} \bar{\mathbf{u}}\bar{\mathbf{u}} : \bar{\mathbf{c}}_i \bar{\mathbf{c}}_i - \frac{1}{2c_s^2} \mathbf{u}^2 \right), \quad (2.7)$$

where $\bar{\mathbf{u}}\bar{\mathbf{u}}$ is the traceless part of $\mathbf{u}\mathbf{u}$, and the double dot product is defined as $\mathbf{A}:\mathbf{B} = \sum_{\alpha,\beta} A_{\alpha\beta} B_{\beta\alpha}$. The weight factors are given by $w_0 = 4/9$, $w_1 = w_3 = w_5 = w_7 = 1/9$ and $w_2 = w_4 = w_6 = w_8 = 1/36$.

In the LB scheme for particulate suspensions as developed by Ladd (1994a), the solid particles are defined by a boundary surface, which can be of any size or shape. The solid particles are placed on the lattice, where the boundary surface cuts some of the links between lattice nodes. Fluid particles moving along the boundary surface interact with the surface at boundary nodes that are located at the lattice nodes nearest to the boundary surface of the solid particles, following an alternative method to Ladd's, that was developed by Behrend (1995). In this method, called relaxed bounce back at the nodes, the LB collisions are carried out at every node, including the boundary nodes. The collision rules at the boundary surface enforce a stick boundary condition on the fluid, which means that the fluid velocity is matched to the local solid-body velocity \mathbf{u}_b . This local solid-body velocity \mathbf{u}_b (at position \mathbf{x}_b) is determined by the solid-particle velocity \mathbf{U} , its angular velocity $\boldsymbol{\Omega}$ and the position of its centre of mass \mathbf{R} :

$$\mathbf{u}_b = \mathbf{U} + \boldsymbol{\Omega} \times (\mathbf{x}_b - \mathbf{R}). \quad (2.8)$$

After the collision phase, the boundary nodes are updated in the following way:

$$f_i(\mathbf{x} + \Delta \mathbf{x}_i, t + \Delta t) = f'_i(\mathbf{x}, t) + \frac{2\rho w_i}{c_s^2} \mathbf{u}_b \cdot \mathbf{c}_i, \quad (2.9)$$

$$f_i(\mathbf{x} - \Delta \mathbf{x}_i, t + \Delta t) = f'_i(\mathbf{x}, t) - \frac{2\rho w_i}{c_s^2} \mathbf{u}_b \cdot \mathbf{c}_i. \quad (2.10)$$

For moving suspension particles, in this update, momentum is exchanged between the incoming particles from the fluid and the solid side (the combined momentum of the fluid and the solid phase is, however, conserved). From this momentum exchange, the force and torque exerted on a suspension particle is calculated. Hereinafter, the

kinematic properties of the suspension particles are updated with a simple Euler forward integration of Newton's second law.

The choice of the location of the boundary nodes, the discretization of the particle surface onto the lattice and the boundary update rules induce a certain hydrodynamic particle diameter that is larger than the diameter based on the number of occupied lattice nodes (Ladd 1994*b*). In dilute systems, in the Stokes flow regime and for sufficiently large particles, the difference between the input particle diameter and the hydrodynamic particle diameter can be considered constant (but dependent on the kinematic viscosity). With the relatively large particle diameters of 16 lattice units applied in this study, this would give a deviation on the input particle diameter of a maximal 5%. In our study, the particle fraction and shear-induced diffusivity are the most important parameters that depend on the particle diameter. A correction method could be to use the hydrodynamic instead of the real particle diameter for the calculation of the particle fraction or shear-induced diffusivity. These calculations are carried out afterwards, so the simulation method itself remains the same. The quadratic dependence of these parameters on the particle diameter would, in its turn, give rise to a maximal deviation of 10% on the particle fraction and the shear-induced diffusivity. In general, this deviation lies within the standard deviation of our simulation results. In our simulations, moreover, we focus on rather concentrated suspensions outside the Stokes flow regime, where we not only expect the deviation to be smaller than for dilute systems in the Stokes flow regime, but also to be dependent on the actual hydrodynamic conditions. Because determination of the actual hydrodynamic diameter in concentrated suspensions outside the Stokes flow regime would become very complex, we used the real particle diameter in our simulations, knowing that this gives a small, probably even negligible error.

Since a suspended particle is essentially simulated by the introduction of a boundary surface, separating the interior of the particle from the exterior, the interior of the particle also consists of fluid. Ladd (1994*b*) examined the effects of the interior fluid on the behaviour of the particle. With a sufficiently high effective mass of the particle, the interior fluid only contributes an inertial force due to the extra mass of the particle. Our computations were carried out in this regime, with an effective mass density ρ_s/ρ of 10. By comparing simulation results with an effective mass of 3 and 10, we found that the relatively high effective particle mass did not contribute to the observed effects of Re_p on the viscosity and shear-induced diffusion in this paper. It can therefore be hypothesized that fluid inertia plays a larger role than particle inertia in our system. This matter is little discussed in the literature, so we do not take it into consideration any further.

Since shear-induced diffusion is mainly governed by hydrodynamic particle interactions, these interactions must be accurately resolved in the computations. When two suspension particles come into close contact with each other, the lubrication force becomes important. This force is caused by the attenuation of the fluid film in the gap between the two particles and is repulsive upon approach and attractive upon separation of the particles. When the gap width between two particles is of the order of one lattice spacing, the lubrication force is, however, not exactly resolved with the LB method. This is due to the discretization of the particles and fluid on a grid and is a problem that is encountered by all numerical methods. To overcome this problem, we applied a lubrication correction as proposed by Ladd & Verberg (2001) for a three-dimensional system. It starts with an explicit calculation of the lubrication force when the gap width is smaller than two lattice units ($= 0.25a$). Since we considered a two-dimensional system, we used the following equation for the lubrication force per

unit length F , which is valid for the lubrication force between two cylinders (see the Appendix):

$$F = \eta U \left(\left(\frac{h}{a} \right)^{-3/2} \left(F_0 + \frac{h}{a} F_1 \right) - \left(\frac{h_c}{a} \right)^{-3/2} \left(F_0 + \frac{h_c}{a} F_1 \right) \right), \quad h < h_c, \quad (2.11)$$

$$F = 0, \quad h > h_c, \quad (2.12)$$

where two particles approach each other with a velocity U , $2h = |\mathbf{R}_{12}| - 2a$ is the gap (distance between the particle surfaces), F_0 and F_1 are numerical constants. In accordance with Ladd & Verberg (2001), we applied a correction on the lubrication force to account for the lubrication force that is already resolved in the computations of the fluid dynamics. This was done by subtracting the lubrication force at a cutoff distance h_c from the total lubrication force, as indicated in (2.11). The cutoff distance h_c represents the cutoff distance between the particle surfaces for the added lubrication force and was chosen equal to one lattice unit ($=0.125a$) in our study. For three-dimensional systems, Nguyen & Ladd (2002) showed that this correction leads to more accurate results for particle interactions at short interparticle distances, even with neutrally buoyant particles very near to contact and without causing instabilities in the particle dynamics. These improvements are also expected for a two-dimensional system.

We have noticed, that in suspensions with particle fractions exceeding 0.40 and at relatively high shear rates, particle clustering and overlap can occur, which greatly affected the diffusive behaviour of the particles. This behaviour seems to be correlated with the lubrication breakdown of concentrated colloids, that was reported by Ball & Melrose (1995). As suggested by these authors, we applied a Hookean spring force between the particles for particle fractions exceeding 0.40 to avoid this clustering and overlap. This Hookean spring force was applied for gaps $2h$ smaller than a thickness δ and was applied in the direction of the line of particle centres, according to:

$$F_h = F_m - \left(\frac{F_m}{\delta} \right) 2h, \quad (2.13)$$

with a maximal Hookean spring force F_m of 10.0 (in lattice units). The Hookean spring force is active in a layer around the particle with a thickness $\delta/2$ of 0.05 lattice units ($=0.00625a$). When using the LB model as described above, we found a good agreement between our computer simulation results for the viscosity and model results of the Krieger–Dougherty model (particle fractions between 0.05 to 0.55). Especially at high particle fractions, the viscosity is known to be highly dependent on particle interactions. The good agreement with the Krieger–Dougherty model therefore indicates that our model captures the particle behaviour well.

3. Effects of hydrodynamics and inertia in particle suspensions

Our simulations on shear-induced diffusion are carried out in a two-dimensional multi-particle suspension (actually cylinders) in a Couette system with solid moving walls. Before examining this complex system, we first studied the behaviour of a single cylinder and of two interacting cylinders in shear flow, in order to investigate some relevant effects in a simpler system. The case of the single cylinder studies wall effects and the effect of Re_p and is compared with data from literature concerning three-dimensional systems. For the case of two interacting cylinders neither analytical nor numerical (two-dimensional) solutions were available so the comparison with

literature is only qualitative. This study is presented to show the effect of Re_p on the flow trajectory of two interacting cylinders in shear flow. Besides these one- and two-cylinder systems, we determined the effects of Re_p on the viscosity of a multi-particle suspension, which enabled us to examine the collective particle behaviour in a Couette system with solid moving walls and relate this behaviour to the results presented in §§4 and 5 of this paper. The results of the preliminary simulations are discussed in this section.

The computer simulations on a single and on two interacting cylinders were carried out in a Couette system, consisting of a box with solid walls at the upper and lower side and periodic boundaries at the left- and right-hand side of the box. The walls move parallel to each other with a constant velocity, but in opposite direction. The width of the box between the periodic boundaries was equal to 640 lattice units ($= 80a$). The height of the box between the two parallel walls was 320 lattice units ($= 40a$) (in most cases) and the wall velocity was between 0.002 and 0.054 lattice units per time step, resulting in a shear rate between 1.25×10^{-5} and 7.50×10^{-4} per time step. Therewith, the shear based particle Reynolds number $Re_{shear,p}$ ($= 4\dot{\gamma}a^2/\nu$, with ν is the kinematic viscosity) was between 0.019 and 1.152. For the case of a single cylinder, the height of the box and the wall velocity were varied, but in such a way that the shear rate and $Re_{shear,p}$ were in the range indicated above.

For a single cylinder placed at the horizontal centreline of the Couette system, the equilibrium angular velocity of the cylinder is determined as a function of the distance between the solid walls and as a function of $Re_{shear,p}$. In this paper, the angular velocity ω is normalized for the shear rate. We compare our results to results of Nirschl, Dwyer & Denk (1995), who carried out comparable computations with a finite-volume numerical scheme, but for a three-dimensional system. Taylor (1932) derived an analytical solution for low-Reynolds-number flow over a rotating sphere in simple shear, which predicts an angular velocity ω of a half. The computed angular velocity ω is presented as a function of $Re_{shear,p}$ in figure 1. For a distance between the walls $Y = 10a$ and $Y = 40a$ and $Re_{shear,p} < 0.5$, the angular velocity ω approached Taylor's solution to within a few per cent. For $Re_{shear,p}$ up to 1.152, no large influence of $Re_{shear,p}$ on the angular velocity ω is seen. The influence was slightly larger for larger distances between the walls. This is in agreement with the findings of Nirschl *et al.* (1995) for a three-dimensional system. The influence of $Re_{shear,p}$ can be attributed to the blockage of fluid near the particle axis. This blockage creates a recirculation of fluid, and the streamlines divert into the gap between the wall and the particle. Therewith the resistance to flow in the gap increases, and the flow losses are larger with increasing $Re_{shear,p}$, leading to a decrease of the angular velocity ω . When the distance between the walls is smaller, the recirculation is inhibited so that the effect of $Re_{shear,p}$ is less than for larger distances. When the distance between the walls decreased to $5a$ or smaller in our simulations, the walls had an increasing effect on the angular velocity ω . Compared to the three-dimensional results of Nirschl and others, this effect is more pronounced in a two-dimensional system. This can be understood because the intensity of the flow field around a cylinder is larger than around a spherical particle.

All together, these results lead us to the conclusion that in the shear regime of our study, $Re_{shear,p}$ does not have a significant effect on the rotation of a single cylinder. When the cylinder closely approaches a solid wall, the angular velocity decreases owing to the interaction with the wall. This effect is larger in a two-dimensional than in a three-dimensional system. These results also give an indication of wall effects in a Couette system where the cylinder is placed eccentrically in that system. It is known

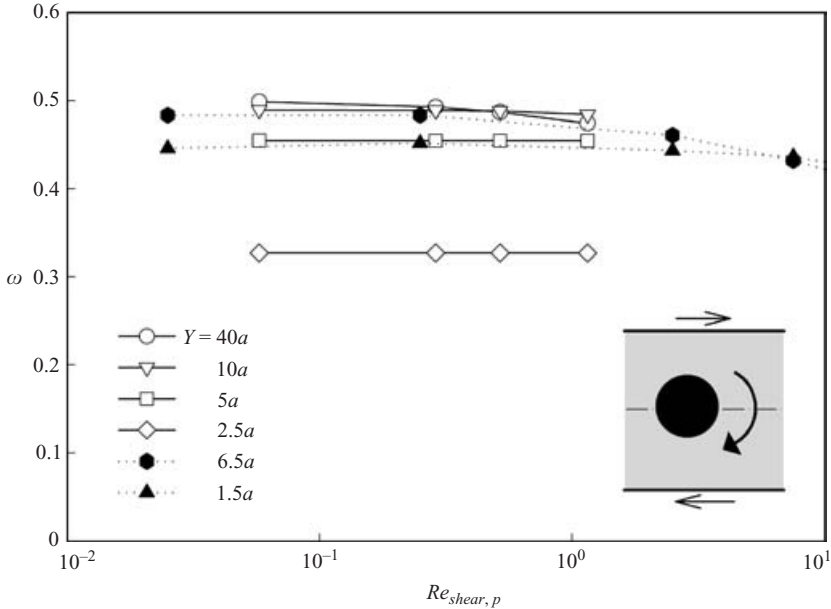


FIGURE 1. The angular velocity ω as a function of $Re_{shear,p}$ for a single cylinder with radius a in shear flow. The distance between the solid walls of the Couette system was varied between 2.5 and $40a$. The results are compared to results of Nirschl *et al.* (1995) for a three-dimensional system (solid symbols). The inset shows a scheme of the simulated situation.

that cylinders tend to migrate to the centreline of a Couette system (Feng, Hu & Joseph 1994b). The migration velocity is, amongst others, dependent on the distance from the wall. We can expect that migration becomes important at particle distances from the wall where the angular velocity is significantly affected. Consequently, when wall effects on the total system need to be negligible, the distance between the walls in a multi-particle system needs to be sufficiently high. Therefore, the distance between the walls was minimally $56a$ in the simulations on multi-particle systems in the rest of this paper.

In another study, we determined the drag coefficient of a single cylinder settling along the centreline of a confined channel (results not shown). These results were found to be in good agreement with results of Feng *et al.* (1994a) and Aidun & Lu (1995), indicating that the drag of a transposing cylinder is accurately resolved with our LB method.

The interactions between two cylinders subjected to simple shear flow provide an important basis for analysing shear-induced diffusive behaviour of suspensions, because this behaviour can be considered the basis for shear-induced diffusion in the low-concentration limit. Batchelor & Green (1972) have derived analytical solutions for three-dimensional systems of spheres without inertia. Trajectories can either extend to infinity (open trajectory) or not (closed trajectory). The interaction between equal-sized spheres is symmetric and such spheres can approach each other to exceedingly small separations. Factors such as surface roughness can disturb the symmetry of the process, because this can impose an additional force onto the spheres when in close contact. Therefore, closed trajectories will probably only occur for very smooth spheres. We have studied the effect of inertia on hydrodynamically interacting

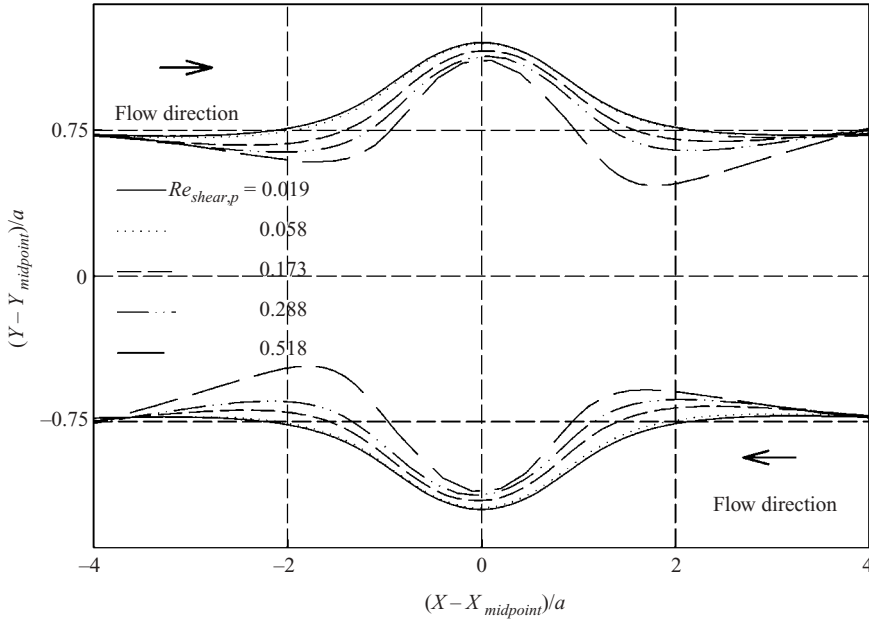


FIGURE 2. Flow trajectories for two interacting cylinders with radius a in shear flow. $Re_{shear,p}$ varied between 0.019 and 0.518. The positions are related to the initial midpoint of the two cylinders.

cylinders by varying $Re_{shear,p}$ in a system with two equal-sized cylinders in an open trajectory.

In our simulations, these two cylinders were placed in the box at heights symmetrical around the horizontal centreline, at a distance of $19.25a$ from the moving wall and $0.75a$ from the centreline. The initial horizontal distance between the cylinders was $10.0a$. Based on the simulations on one cylinder as presented in figure 1, it can be expected that the walls did not affect the flow of the cylinders. The trajectories of the interacting cylinders were computed for various shear rates (figure 2).

At a $Re_{shear,p}$ of 0.019 and 0.058, no clear effects of inertia can be seen in the flow trajectories. In their tumbling movement around each other, the cylinders reach a minimum separation of $0.20 \times 2a$ (figure 3). When compared to three-dimensional systems, this minimum separation is large. This can be explained because the flow of fluid out of (into) the gap during approach (separation) of two parallel cylinders is more hindered than for the case of spheres. The trajectories upon approach and upon separation are practically symmetric, which is in accordance with the relatively large separation distances in this system. At $Re_{shear,p} > 0.058$, inertial effects become visible in the trajectories. One effect is that the separation distance between the cylinders became smaller, both during approach and during separation. The minimum separation between the cylinders decreased to $0.11 \times 2a$ for $Re_{shear,p}$ equal to 0.52 (figure 3). This effect can be explained because inertia causes the cylinders to move to different streamlines, and is probably due to particle inertia rather than fluid inertia. A second effect is that at larger separation distances, the cylinders slowly moved towards the centre axis of the system before they start tumbling over each other. Upon separation, a similar movement away from the centre axis took place. Inertial effects in the fluid flow around the cylinders are the most probable cause for this effect. Finally, the trajectories upon approach and separation exhibited an

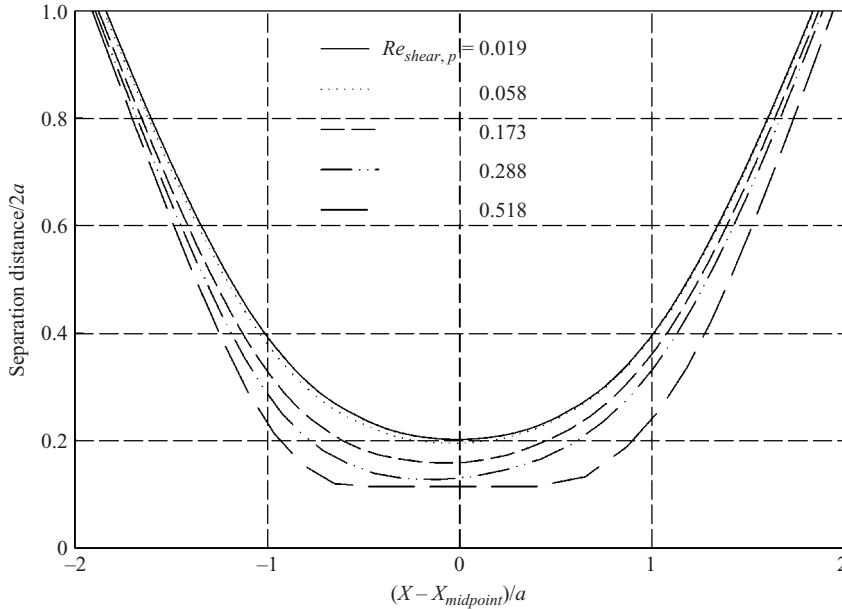


FIGURE 3. Separation distance as a function of the horizontal position of the upper cylinder, for two interacting cylinders with radius a in shear flow. $Re_{shear,p}$ varied between 0.019 and 0.518.

increasing asymmetry with increasing $Re_{shear,p}$. This effect, although small, can be seen in figure 3. The minimum separation was still too large to be able to explain the observed asymmetry with the action of the repulsive Hookean spring force F_h or with the effect of surface roughness (a different flow trajectory would then also be expected). Inertial effects seem, therefore, to be responsible for this asymmetry. The inertial effects during the interaction between the cylinders lead to a dispersal of the cylinders at $Re_{shear,p} = 0.52$, which proceeded with repeated encounters of the cylinders (figure 4). Even when the separation distance between the cylinders has become larger than $7 \times 2a$, the dispersal still proceeds. Because the vertical velocity decreases with increasing separation distance and does not exhibit a logarithmic trend in time, it is expected that the cylinders will have reached their equilibrium position at a separation distance of about $8 \times 2a$. The distance from the walls was still about $12a$, so that it is not likely that this final separation distance is affected by the presence of the walls.

The viscosity is determined from a multi-cylinder suspension in a Couette system, with $Re_{shear,p}$ varying between 0.003 and 0.33. Our results for the viscosity are presented as relative values to results from the semi-empirical model of Krieger & Dougherty (Krieger & Dougherty 1959; Krieger 1972). This model is known to give accurate predictions for the viscosity at low Re , for both two- and three-dimensional suspensions. The effective viscosity μ_s/μ_f is calculated as follows:

$$\mu_s/\mu_f = \left(1 - \frac{\langle\phi_s\rangle}{\phi_{max}}\right)^{-[\eta]\phi_{max}}, \quad (3.1)$$

where $\langle\phi_s\rangle$ is the averaged solid volume or area fraction and ϕ_{max} is the maximum packing fraction, which has a value of 0.82 for a two-dimensional suspension. The dimensionless factor $[\eta]$ is the intrinsic relative viscosity of the suspension and has a value of 2 for a two-dimensional suspension.

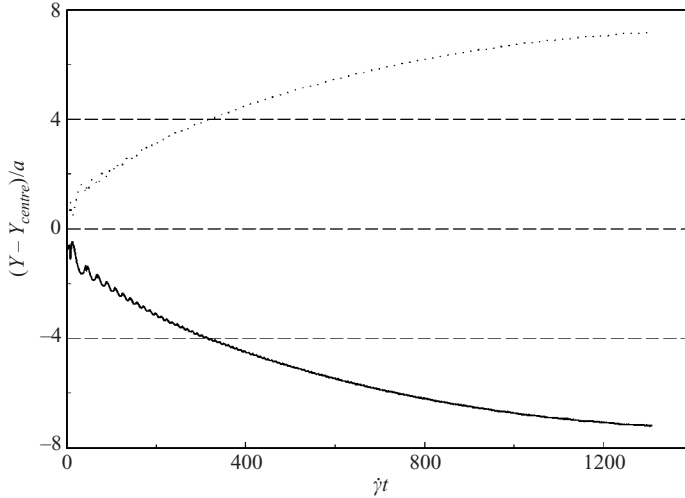


FIGURE 4. Vertical position $(Y - Y_{centre})/a$ as a function of the strain $\dot{\gamma}t$ for two interacting cylinders with radius a in shear flow. $Re_{shear,p}$ was equal to 0.518. The initial position of the cylinders was symmetrical around the centre axis, at a distance of $0.75a$ from the centre axis and of $19.25a$ from the nearest wall. The oscillations in the trajectory are caused by the repeated encounters of the cylinders.

In our computations, the system height and width were $518 (=64.75a)$ and $259 (=32.38a)$ lattice units, respectively, and the shear rate varied between 1.93×10^{-6} and 2.16×10^{-4} per time step. An amount of 66, 166 or 266 cylinders with radius a were randomly suspended in the domain, corresponding with area fractions ϕ of 0.10, 0.25 and 0.40, respectively. The viscosity was determined from the average stress at the walls over a strain range of at least 1.5 at a shear rate of 1.93×10^{-6} per time step, increasing to a strain range of 86 at a shear rate of 2.16×10^{-4} per time step. This increase of strain range was necessary to acquire sufficient accuracy at high shear rates, where the time-dependent fluctuations of the stress were higher.

Our viscosity data in the regime with low $Re_{shear,p}$ agree well with the Krieger–Dougherty model (figure 5). At higher $Re_{shear,p}$, however, starting at $Re_{shear,p} = 0.012$, shear thickening occurred in the suspensions with area fractions of 0.25 and 0.40. This shear thickening was most intense at an area fraction of 0.40, where the effective viscosity increased by about 35% with an increase of $Re_{shear,p}$ to a value of 0.1. At these high values for $Re_{shear,p}$, the viscosity starts to levels off. The velocity profile in the Couette system was found to be linear, except for $\phi = 0.40$ and $Re_{shear,p} > 0.2$, where slip started to occur near the wall. At $\phi = 0.40$ and $Re_{shear,p} = 0.33$, this led to a decrease of the shear rate in the bulk phase of about 15% when compared to a situation with a linear profile. This might also have consequences for the accuracy of the viscosity calculations, since the viscosity is determined from the stress near the wall. For the great majority of the calculations, however, slip did not play a role and the viscosity calculations are expected to be accurate. For highly concentrated suspensions, the increase of viscosity with increasing particle fraction in the Stokes flow regime has been found to coincide with particle clustering (Brady & Bossis 1985). It might be that in our case, where we found a viscosity increase with shear rate, particle clustering also plays a role. An analysis on particle clustering in our system is therefore presented in § 5.

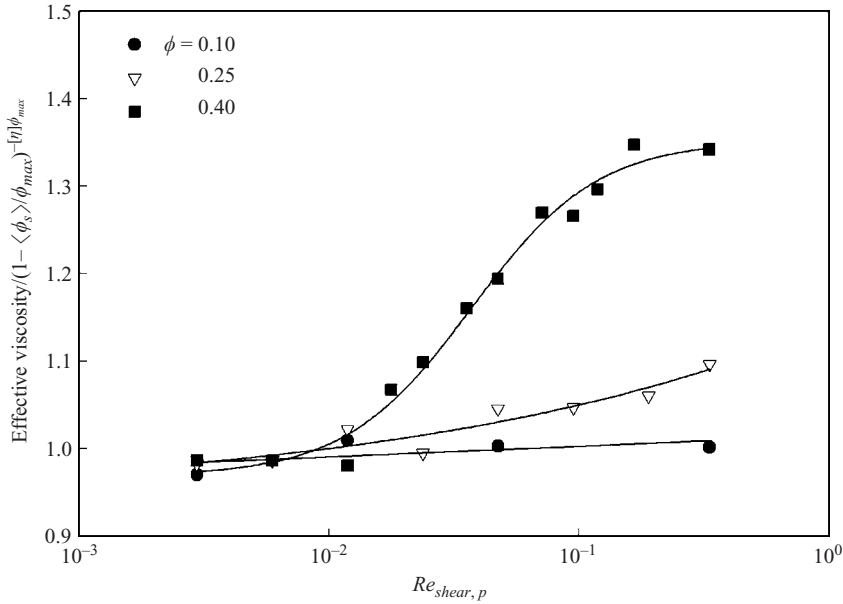


FIGURE 5. Viscosity of a two-dimensional suspension as a function of $Re_{shear,p}$ for suspensions with an area fraction cylinder ϕ of 0.10, 0.25 and 0.40. The viscosity is presented as the effective viscosity, normalized for model results of the Krieger–Dougherty model ($\phi_{max} = 0.82$, $[\eta] = 2$) at the respective area fractions. The lines are fits to the data points and are drawn as a guide to the eye.

Although limited results are available, shear thickening behaviour has also been observed by other workers, experimentally as well as in computer simulations (see e.g. Hoffman 1998; Shakib-Manesh *et al.* 2002). Shear thickening is found particularly in suspensions where hydrodynamic forces are dominant (at high Péclet number ($= 8\mu_f a^3 \dot{\gamma} / kT$ where k is the Boltzmann constant and T the absolute temperature)). Similar to our results, Shakib-Manesh *et al.* (2002) observed shear thickening of two-dimensional suspensions. In their study, for suspensions with a cylinder area fraction up to 0.52, the effect of shear thickening on the viscosity was only relevant when $Re_{shear,p}$ was larger than about 0.5, so, in a quantitative sense, their results do not fully agree with ours. This may, however, be due to differences in the way the particle interactions are handled at short distances in the codes used. In contrast to our method, Shakib-Manesh *et al.* did not correct for the lubrication force at short particle distances; this difference might be relevant for clustering behaviour of the suspension. This comparison shows that shear thickening can be delicately affected by interparticle forces, which hampers quantitative comparison of data.

4. Shear-induced diffusion at non-zero Reynolds numbers

In this section, we present results of LB simulations on shear-induced diffusion in two-dimensional systems. In these two-dimensional systems, we can distinguish components of the shear-induced self-diffusion tensor in the fluid velocity and in the velocity gradient direction, and their diagonal component. Whereas the displacements in the velocity gradient direction are purely determined by the hydrodynamic interactions between the cylinders, the displacements in the fluid velocity direction also consist of a convective term due to the shear flow of the fluid. The analysis of

shear-induced self-diffusion in the velocity gradient direction is consequently more straightforward. Since the component in the velocity gradient direction is, in practice, the most relevant, we only describe our results for this direction.

The relevant time and length scales in the system are the shear rate $\dot{\gamma}$ and the cylinder radius a , respectively. On basis of dimensional arguments, it can be shown that the self-diffusivity scales as $\dot{\gamma}a^2$ (in the Stokes flow regime). All diffusivities reported are therefore normalized on $\dot{\gamma}a^2$.

The shear-induced self-diffusion coefficients can be determined from the increase of the mean-square displacements with time after diffusive motion has been established, according to:

$$\langle y(t)y(t) \rangle \approx 2D_{yy}t. \quad (4.1)$$

The angle brackets denote an average over all cylinders in the system, while y denotes the displacement of a single particle in the direction of the velocity gradient. D_{yy} denotes the self-diffusivity in the velocity gradient direction. This self-diffusivity is defined as the time rate of change of a half multiplied by the mean-square displacement:

$$D_{yy} \equiv \lim_{t \rightarrow \infty} \frac{1}{2} \frac{d}{dt} \langle y(t)y(t) \rangle. \quad (4.2)$$

The motion of a non-Brownian cylinder is, in principle, purely deterministic and the displacement of a given cylinder depends only on the external velocity field and its interactions with all other cylinders in the system. To obtain the random displacements that are a characteristic of diffusive motion, the initial cylinder configuration must also be changed. As a consequence, the sampling time must be relatively long in order to determine the diffusion coefficients. Therefore, shear-induced diffusion can be characterized as a long-time diffusion process.

As for the aforementioned studies on one or two interacting cylinders in shear flow and on the viscosity in relation to the particle fraction, the system consisted of a Couette system with periodic boundaries in the flow direction of the fluid and two moving walls in the velocity gradient direction. A varying number of cylinders with a radius of 8 lattice units is randomly distributed in the system at the start of the simulation. The simulation runs were started with position-dependent fluid and cylinder velocities according to linear shear flow.

As an example of the typical time-dependent behaviour of the cylinder displacements, in figure 6, a mean-square displacement curve is shown for a system with a cylinder number N of 200 and an area fraction ϕ of 0.25. From the double-logarithmic plot in figure 6, it becomes clear that, at very short times, the mean-square displacement shows a quadratic temporal behaviour, which corresponds to the deterministic strongly correlated cylinder displacements in this regime. Only after a strain of about $\dot{\gamma}t = 8$ do the cylinder displacements become random, resulting in a linear behaviour of the mean-square displacement curves. The diffusion coefficient, which is evaluated from this simulation run, is also given in figure 6. In order to evaluate the effect of the initial particle configuration on the diffusion coefficient, we split the displacement curve of one simulation run into several curves which start at different times of the simulation run (and consequently at different particle configurations). In each separate curve, the mean-square displacement was monitored over a strain of 30. The final diffusion coefficient is the mean value of the diffusion coefficients that were determined from the individual mean-square displacement curves.

From a strain $\dot{\gamma}t$ of about 1 to 8, a transitional regime exists, in which the temporal behaviour is neither quadratic nor linear. Although this is not necessarily

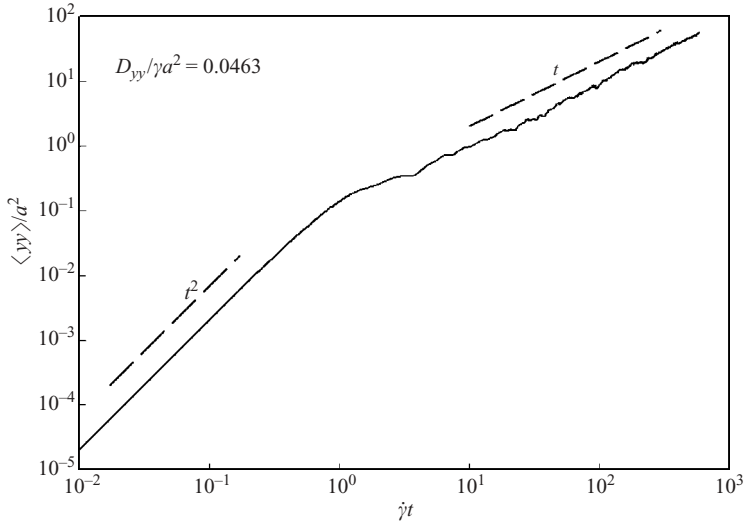


FIGURE 6. Mean-square displacement in the velocity gradient direction as a function of time, both presented as dimensionless values, for a two-dimensional suspension ($N = 200$, $\phi = 0.25$) in shear flow at $Re_{shear,p} = 0.023$.

true, the time-dependent behaviour in our (two-dimensional) simulations compares well with the findings of Sierou & Brady (2004) from their (three-dimensional) ASD simulations. Our results confirm their statement that strains must be sufficiently long in order to obtain an accurate value for the shear-induced diffusion coefficient. Strains that are too small lead to an overestimation of the shear-induced diffusion coefficients. This probably explains the relatively high diffusion coefficients in some experimental studies, e.g. the study of Breedveld *et al.* (2001).

The number of cylinders in the system is known to be an important factor in the determination of the diffusion coefficients (Sierou & Brady 2004). The main reason for this is that for cylinder separations greater than the length of the system, the cylinders can interact with their periodic images, which affects the diffusivities. Smaller cylinder numbers correspond with a smaller system size, which might lead to a larger deviation in the calculated diffusivity. For concentrated suspensions, it can be expected that this deviation depends more on the cylinder number than on the system size (in other words, at higher concentrations, smaller system sizes would suffice). In our system, this idea is only relevant for the velocity direction, since we have no periodic boundaries in the velocity gradient direction. Because the number of cylinders that is sufficient for an accurate calculation of the diffusivity cannot be theoretically evaluated, it needs to be established in an empirical way. Therefore, in figure 7, the calculated diffusion coefficients are presented as a function of the number of cylinders for an area fraction ϕ of 0.25. To investigate the effect of the number of cylinders, only the width X of the simulation box was varied, while the height Y between the confined walls was kept constant at $71a$. For cylinder numbers smaller than $N = 100$, there is a rather sharp increase in diffusivity with the number of cylinders. This is followed by a levelling off of the diffusivity with higher numbers of cylinders. The decrease of the standard deviation from $N = 200$ to $N = 600$ reflects the improved statistical accuracy by the increased cylinder number, since the same number of configurations is used for the calculation of shear-induced diffusivity. From the observed relationship, we draw the conclusion that a cylinder number of more than 100 is required for the

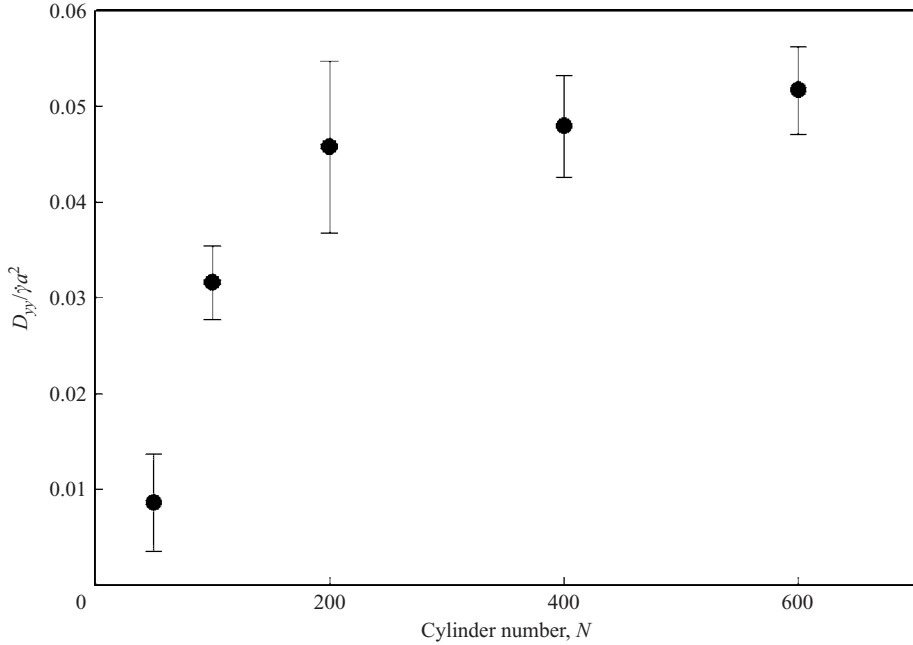


FIGURE 7. Component D_{yy} of the shear-induced self-diffusion coefficient as a function of the cylinder number N for a two-dimensional suspension ($\phi = 0.25$) in shear flow at $Re_{shear,p} = 0.023$. The width of the simulation box between the periodic boundaries is varied, while the height between the confined walls is kept constant at $71a$. The error bars indicate the standard deviation of the mean shear-induced self-diffusion coefficient, which is determined from 6–12 individual mean-square displacement curves with different initial particle positions and over a strain of 30.

determination of diffusivities with sufficient accuracy. Since the box dimensions at an equal particle number differ for a two-dimensional and a three-dimensional system, it can be expected that the dependence of shear-induced diffusivity on the particle number is also different. However, the relation between the diffusivity and the cylinder number is found to compare well with the one that was found in SD simulations for three-dimensional systems (Sierou & Brady 2004). Our results therewith confirm a statement of Sierou & Brady (2004), namely that the results of Foss & Brady (1999) are influenced by the fact that they only used a particle number N of 27 in their SD simulations. For the following simulations presented in this paper, we applied a cylinder number N of 200, unless otherwise stated. The size of the simulation box is chosen such that Y was always twice as large as X , as is the case in the simulations presented in figure 7 with $N = 200$. The distance between the solid walls Y was such that the measured shear-induced diffusivity agrees with that of an infinitely large system (results not shown).

LB simulations are not limited to the Stokes flow regime. This makes it possible to determine the particle movements in systems with non-zero Reynolds numbers, which can be considered relevant for many practical systems. During pipeflow and microfiltration for example, the shear rate can, in general, easily exceed values of 1000 s^{-1} , which is already beyond the Stokes flow regime for suspensions with particles sizes in the micrometre range. On the basis of the consideration that particle interactions cause shear-induced diffusion and that the number of particle interactions scales linearly with the shear rate, it can be expected that the dimensionless diffusion

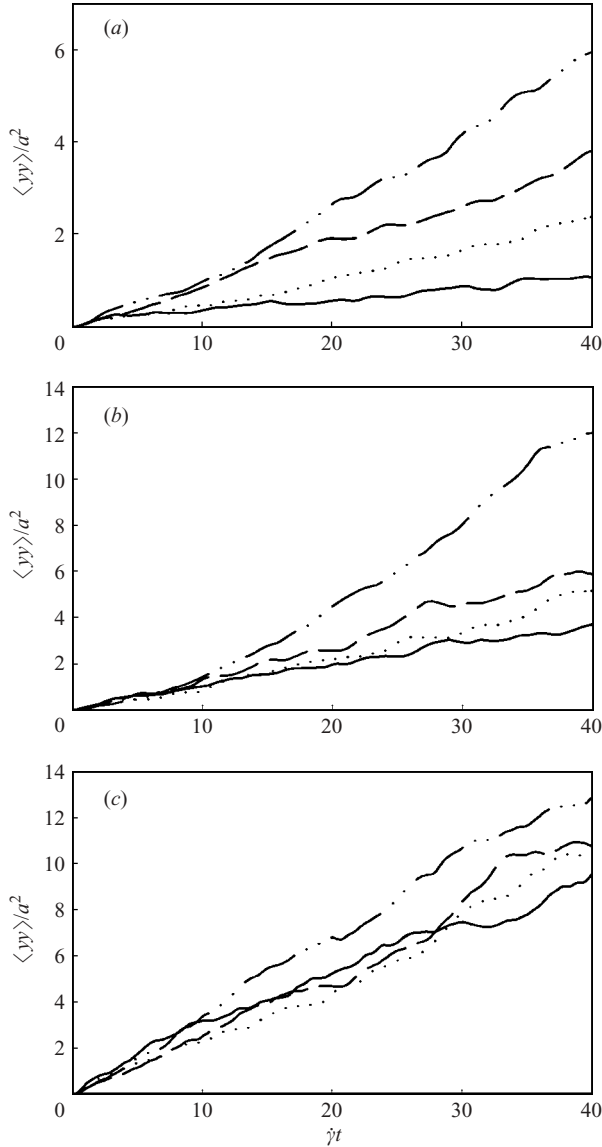


FIGURE 8. Mean-square displacement in the velocity gradient direction as a function of time, both presented as dimensionless values, for a two-dimensional suspension ($N = 200$, (a) $\phi = 0.10$, (b) 0.25 and (c) 0.40) in shear flow at $Re_{shear,p} = 0.023$ (solid line), 0.115 (dotted line), 0.161 (medium dashed line) and 0.346 (dash-dot-dotted line).

coefficient $D_{yy}/\dot{\gamma}a^2$ is independent of $\dot{\gamma}$ in the regime where inertial or other shear-related effects do not (yet) play a role. To our knowledge, however, it is not known at which conditions inertial or other shear-related effects come into play and how they affect shear-induced diffusion. We therefore analysed the particle movements in the velocity gradient direction in relation to $Re_{shear,p}$.

For $Re_{shear,p}$ from 0.023 up to 0.346 and cylinder area fractions of 0.10 , 0.25 and 0.40 , the mean square displacement $\langle yy \rangle / a^2$ as a function of the strain $\dot{\gamma}t$ is presented in figure 8. The relation was linear (after a strain $\dot{\gamma}t \approx 8$), as in accordance with shear-induced diffusive behaviour. We also observed that the average displacement

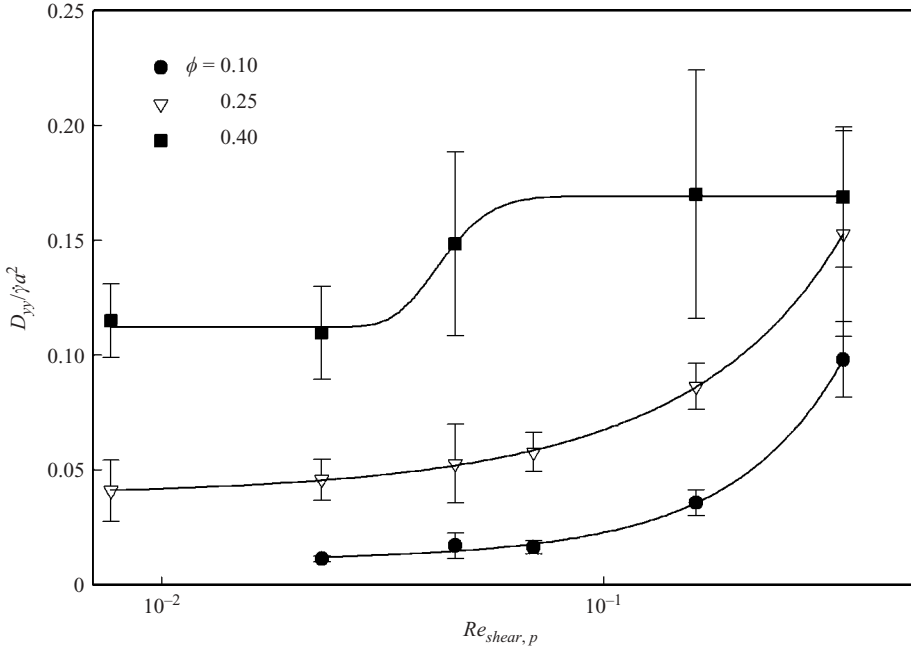


FIGURE 9. Component D_{yy} of the shear-induced self-diffusion coefficient as a function of $Re_{shear,p}$ for a two-dimensional suspension ($N = 200$) in shear flow with a cylinder area fraction ϕ of 0.10 (filled circles), 0.25 (open triangles) and 0.40 (filled squares). The error bars indicate the standard deviation of the mean shear-induced self-diffusion coefficient, which is determined from 6–12 individual mean-square displacement curves with different initial particle positions and over a strain of 30. The lines are fits to the data points and are drawn as a guide to the eye.

in the velocity gradient direction remained (nearly) zero for particle area fractions of 0.10, 0.25 and 0.40. The particle distribution across the height between the two walls remained nearly constant in time as well, which also indicates that no net particle transport has taken place. At a cylinder area fraction of 0.10 and 0.25, however, a systematic increase of $\langle yy \rangle / a^2$ with $\dot{\gamma}t$ is observed when $Re_{shear,p}$ was increased. At a cylinder area fraction of 0.40, this increase with $Re_{shear,p}$ was also present, although not as evident as for an area fraction of 0.10 and 0.25. The diffusivity seems to reach a plateau value at this area fraction of 0.40. As mentioned in §3, wall slip starts to occur at $\phi = 40$ and for $Re_{shear,p} > 0.2$. The effect of wall slip on the shear rate seems too small to explain the relatively small increase of the diffusivity at $\phi = 40$, but the behaviour might be related to microstructural features. This is investigated in the next section.

The results indicate that the dimensionless diffusion coefficient $D_{yy}/\dot{\gamma}a^2$, as determined from the slope of the curves in figure 8, was not independent from the shear rate, as is shown in figure 9. For $\phi = 0.10, 0.25$ and 0.40, the increase started at about $Re_{shear,p} = 0.04$, which is comparable to where the shear thickening behaviour started. The effect of the cylinder fraction was, however, opposite between shear-induced diffusion and viscosity, because we observed the largest effects on shear-induced diffusion at the lower cylinder fractions.

In spite of the lower number of particle collisions, the standard deviation of the shear-induced diffusivity was relatively low at a particle area fraction $\phi = 0.10$. This

indicates that, in principle, the averaging took place over sufficiently large strains and with sufficiently high cylinder numbers. The standard deviation, however, increased with increasing $Re_{shear,p}$ and when $D_{yy}/\dot{\gamma}a^2$ exceeded a value of about 0.10, the standard deviation was relatively large, indicating time-dependent fluctuations in the collective cylinder movements. This might be a combined effect of correlated movement of the cylinders, caused by particle clustering, and high stresses on the cylinders. Improving the accuracy of the shear-induced diffusion coefficients in this regime would require much larger systems, which was not deemed necessary in this study.

It may be expected that the dependence of the shear-induced diffusivity on $Re_{shear,p}$ is due to the correlated motion of cylinders, in other words, to the formation of a suspension microstructure. In the next section, this microstructure is analysed in order to have a clearer picture of shear-induced changes in the suspensions.

5. Shear-induced changes in microstructure

In order to analyse the microstructure, we determined the two-dimensional pair-distribution function, which represents the concentration distribution of cylinders around a cylinder. This pair-distribution function was assessed by averaging the pair-distribution function of two separate simulation runs. In each simulation run, the distribution function was determined by averaging the distribution at five different strains, namely at $\dot{\gamma}t = 30.0, 37.5, 45.0, 52.5$ and 60.0 . Cylinders at a position closer than a distance $0.2Y$ ($Y =$ height between the walls) from the wall were excluded as reference particles from the distribution function, in order to avoid wall effects. The concentration distributions are only shown for ΔX and ΔY smaller than $3.5a$, because outside this region no cylinder preference positions could be observed. For a cylinder area fraction of 0.10, a clear effect of $Re_{shear,p}$ can be seen (figure 10). At $Re_{shear,p} = 0.023$, a concentration peak can be observed above and under the cylinder, at a distance of about $2a - 3a$. The concentration distribution was anisotropic as no peak can be observed left and right of the particle. At higher $Re_{shear,p}$, the concentration peak at a distance of about $2a - 3a$ becomes more circular (isotropic) as well as more pronounced. A maximum concentration peak with a value of about 1.4 a.u. is found at $Re_{shear,p} = 0.161$. These results clearly show that the cylinders tend to stay closer to each other at higher $Re_{shear,p}$. For a cylinder area fraction of 0.25, already at $Re_{shear,p} = 0.023$ a circular concentration peak was present at a distance of about $2a - 3a$ (figure 10). Small peaks with a maximum concentration of about 2.8 a.u. were already present as well. With increasing $Re_{shear,p}$, the concentration peak was more pronounced, which again indicates an increased clustering of the particles. The concentration profile at a cylinder area fraction of 0.40 was already very pronounced at $Re_{shear,p} = 0.023$ with locally maximum concentrations of about 5.0 a.u. (figure 10). In contrast to cylinder area fractions of 0.10 and 0.25, high $Re_{shear,p}$ did not, however, invoke more clustering. This seems to be consistent with the effects on shear-induced diffusion, where we also found minor changes at a cylinder area fraction of 0.40.

In the pair-distribution function, the concentration peaks at short interparticle distances are generally very high, whereas they are less pronounced at longer interparticle distances, especially in the case of isotropic distributions. This makes the pair-distribution function less sensitive to concentration variations at longer interparticle distances and therefore not suited for the analysis of the size and density of the particle clusters. These parameters can, however, be determined from the scaling of the integrated pair correlation function, according to a version of the so-called

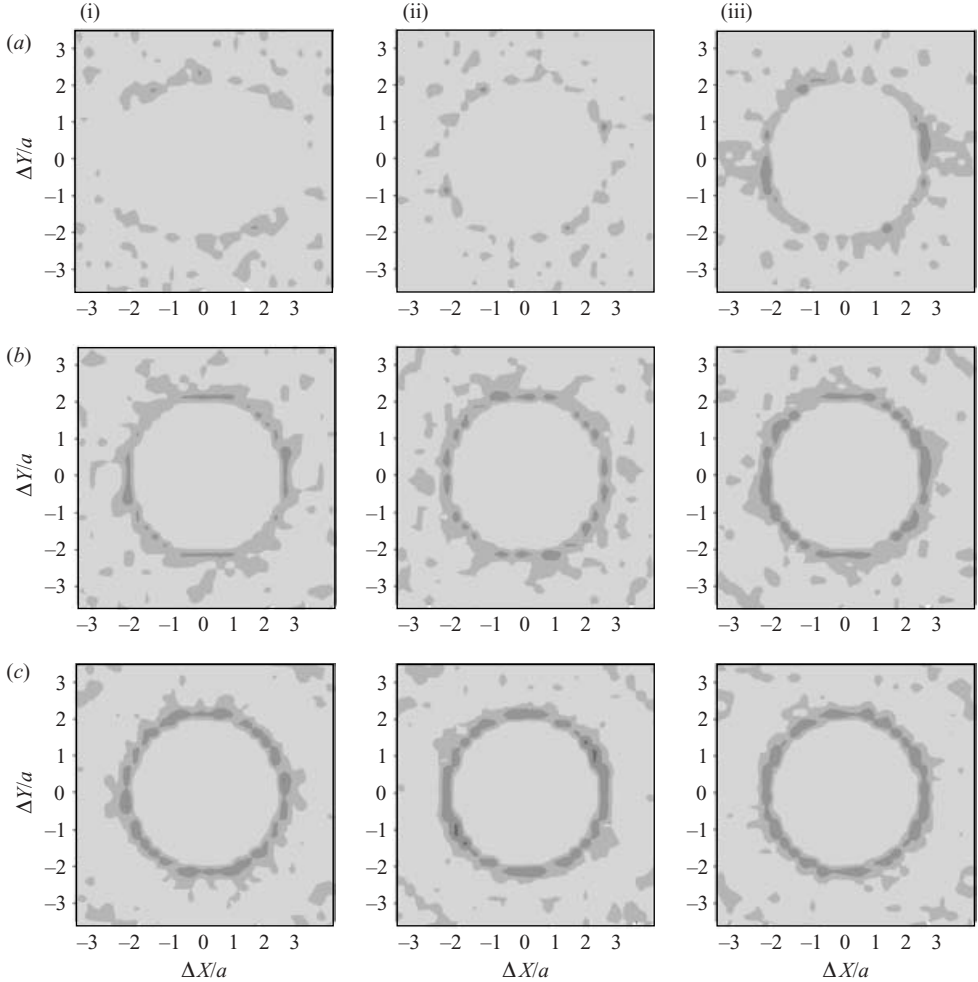


FIGURE 10. The two-dimensional pair-distribution function, averaged over a strain γt from 30 to 60, for a two-dimensional suspension ($N = 200$) in shear flow with a cylinder area fraction ϕ of (a) 0.10, (b) 0.25 and (c) 0.40 at (i) $Re_{shear,p} = 0.023$, (ii) 0.161 and (iii) 0.346. Dark regions represent high probability and light, low probability.

sandbox method (Haw, Poon & Pusey 1994). In this method, we consider the number of particles $n(r)$ in a sphere of radius r around any particle of the cluster. Simple linear regression on $\log(n)$ versus $\log(r)$ yields the parameters n_0 and d_f from the scaling relation for fractal clusters:

$$n(r) = n_0 \left(\frac{r}{a} \right)^{d_f}, \quad (5.1)$$

where n_0 is a dimensionless proportionality constant (generally of order unity, the actual value of n_0 depends on the definition of r used) and d_f is the fractal dimensionality. In a plot of $\log(n)$ versus $\log(r)$, we would see a fractal regime for low values of r which ends at the size of the average cluster in the system (we have neglected effects of monomers, which have zero close neighbours and hence suppress n_0). At high values of r we have the homogeneous regime, where the number

of neighbouring particles simply scales with the volume of the surrounding sphere. The prefactor then becomes the volume fraction:

$$n(r) = \phi \left(\frac{r}{a} \right)^3 \quad (5.2)$$

In our two-dimensional system, the number of neighbouring cylinders scales with the area of the surrounding cylinder, which changes the power in this equation from 3 to 2. If the fractal regime extends all the way to the homogeneous regime, there is an intersection point between the two regimes. The radius which corresponds to this intersection point is called the correlation length ζ and is an indication of the average size of the aggregates. In many systems, however, there will be a finite cross-over regime between the fractal and homogeneous regime, which can, for example, be due to the existence of clusters of various sizes and shapes. In this case, the correlation length can be defined by linear extrapolation of the fractal and homogeneous scaling regime to the intersection point.

In our results, from a distance of $5a - 10a$, the regime is indeed found to be homogeneous (figure 11). The regime is clearly non-homogeneous for smaller distances, but the slope varies with the distance. This indicates that aggregates are present, but that the fractal dimensionality varies with the distance from the centre of the aggregate. The averaged size of the aggregates can be obtained from the point where the non-homogeneous regime turns into the homogeneous regime; a constant fractal dimensionality is not required. Therefore, the correlation length was assessed by determining the distance r/a where the fit value, obtained by linear regression of the $\log(n(r)) - \log(r/a)$ -plot at distances r/a larger than 10, deviated more than 5% from the actual value of $\log(n(r))$. These data are also given in figure 11. The correlation length is found to depend on the area fraction cylinders in the system as well as on $Re_{shear,p}$. The lowest correlation length of $2.3a$ is found for an area fraction of 0.40 and $Re_{shear,p} = 0.023$. For area fractions of 0.10 and 0.25, the correlation lengths were $4.0a$ and $3.9a$, respectively ($Re_{shear,p} = 0.023$). With increasing $Re_{shear,p}$, the correlation length tends to increase, to maximal $7.5a$, $6.9a$ and $5.3a$ for area fractions of 0.10, 0.25 and 0.40, respectively. The largest clusters are again found at the lowest area fraction.

Compared to the pair-distribution functions, these results provide additional information about the size of the clusters. The results agree well with each other; the largest effects of $Re_{shear,p}$ on the microstructure are found for the lowest area fractions. Moreover, the trends in the effects of $Re_{shear,p}$ on the microstructure agree well with the effects on shear-induced diffusion. It seems likely that the microstructure is the coupling factor for the effect of $Re_{shear,p}$ on shear-induced diffusion. The development of particle clustering might, moreover, be related to the longer and closer approach of two interacting particles at higher shear rates. This direct relationship with microstructure does, however, not exist for the viscosity of the suspension, where not only the microstructure seems to be important, but also the averaged solid volume fraction, resulting in a more pronounced effect of $Re_{shear,p}$ at high area fractions (Shakib-Manesh *et al.* 2002). Because of the direct coupling between microstructure and shear-induced diffusion, it can be expected that other factors that can affect the microstructure, such as attractive colloidal forces between the particles, will also affect shear-induced diffusion.

In our results, $Re_{shear,p}$ starts to have a significant effect on the shear-induced diffusivity at a value of about 0.1. In practical systems, for a suspension with particles

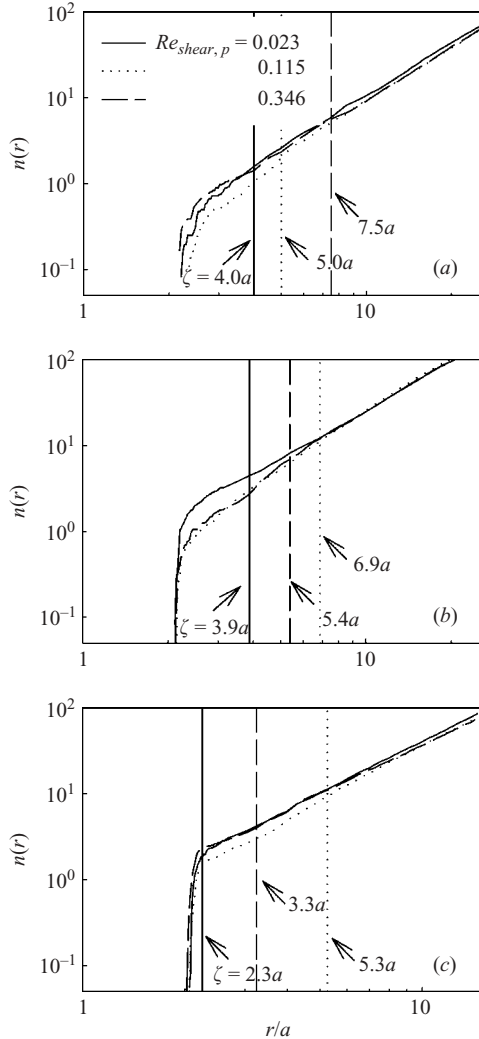


FIGURE 11. The number of cylinders $n(r)$ contained in a circle of radius r for a two-dimensional suspension in shear flow with a cylinder area fraction of (a) 0.10, (b) 0.25 and (c) 0.40 at $Re_{shear,p} = 0.023 - 0.346$. The values are time-averaged over a strain $\dot{\gamma}t$ from 30 to 60. The correlation length ζ represents the distance where the cylinder distribution changes from non-homogeneous into homogeneous.

with a radius a of $3\ \mu\text{m}$, for example, a shear rate of about $2800\ \text{s}^{-1}$ would be required in order to obtain this significant effect. For larger particles, this value quickly drops down to even lower values. The shear rate in this example is well within the range of commonly applied shear rates, which indicates the relevance of this study to practical systems.

6. Conclusions

In this study, the LB method was applied in order to examine the effects of shear rate on the flow behaviour and microstructure of non-Brownian suspensions in a Couette system. In the shear regime studied, inertial effects on a single cylinder were

negligibly small. In a system with two interacting cylinders, however, some effects of the shear rate were present. First, the cylinders approached each other more closely and during a longer time with increasing shear rate, which is in accordance with expectations when inertia causes them to move to other streamlines. Secondly, at $Re_{shear,p}$ higher than 0.06, the particle trajectory started to become asymmetric, finally leading to a dispersal of the two particles. The viscosity was also dependent on the shear rate in the shear regime studied: the suspension namely exhibited shear thickening behaviour.

In order to know how we could reliably evaluate shear-induced self-diffusion in our system, first, the displacements of the particles were monitored as a function of strain. The simulations clearly showed that shear-induced self-diffusion is a long-time diffusive behaviour, which typically only established itself after a strain of about 5–10. Furthermore, it is shown that at least a few hundred suspended particles are needed in the simulations to resolve shear-induced diffusion coefficients reliably. For systems with fewer than 100 particles, the suspended particles interact with their periodic images over the periodic boundaries in the system, leading to an underestimation of the diffusion coefficients.

Following the developed method, the effect of $Re_{shear,p}$ up to 0.35 on shear-induced self-diffusion was investigated for particle fractions of 0.10, 0.25 and 0.40. In contrast to theory for the Stokes flow regime, which predicts a linear increase of the diffusivity with shear rate, the mean square particle displacements were found to increase faster at increasing $Re_{shear,p}$, leading to an increase of the dimensionless shear-induced diffusion coefficient $D_{yy}/\dot{\gamma}a^2$. This increase was most pronounced at particle fractions of 0.10 and 0.25 and started already at $Re_{shear,p}$ equal to 0.05–0.07, which is comparable to the shear regime where effects on two interacting particles and the viscosity arose.

Analysis of the microstructure of the suspensions revealed that an increase of $Re_{shear,p}$ leads to an increase of particle clustering, especially at particle fractions of 0.10 and 0.25. The effects of $Re_{shear,p}$ on particle clustering relate well to the effects on shear-induced diffusion, indicating that the microstructure of suspensions is a key factor for shear-induced diffusivity. This will have consequences for suspensions with attractive interparticle forces.

Friesland Foods is greatly acknowledged for supporting this research. Professor Mike Cates and Dr Kevin Stratford from Edinburgh University as well as Dr Joost van Opheusden from Wageningen University are greatly thanked for fruitful discussions. The authors would like to acknowledge the support of the Dutch Ministries of Economic Affairs, Education, Culture and Sciences and of Housing, Spatial Planning and the Environment through a grant of the Dutch Program Economy, Ecology and Technology and the support of the European Commission through grant number HPRI-CT-1999-00026 (the TRACS Programme at EPCC).

Appendix. Lubrication force in a two-dimensional suspension

We apply lubrication theory to calculate the hydrodynamic force between two cylinders in a two-dimensional suspension. For small gaps (i.e. rim to rim distances) $2h$ the force between two adjacent cylinders can be calculated, solving the flow field in the gap upto first order in $\epsilon = h/a$. In the calculation, two cylinders are considered, approaching each other with a velocity $2U$. A Cartesian coordinate system (e_x, e_z) was used with the origin at the centre of the gap. The z -coordinate, taken along the line of centres, was scaled on h and the x -coordinate was scaled on \sqrt{ah} ; the

z -component of the velocity was scaled on U , the x -component on $\sqrt{a/h}U$. The pressure was scaled on $a\eta U/h^2$. Under these conditions, the differential equation for the dimensionless streamfunction ψ becomes:

$$\frac{\partial^4 \psi}{\partial z^4} + 2\epsilon \frac{\partial^4 \psi}{\partial x^2 \partial z^2} + \epsilon^2 \frac{\partial^4 \psi}{\partial x^4} = 0. \tag{A 1}$$

The rim of both disks is described by $z = \pm b(x)$ with

$$b(x) = 1 + 12x^2 + \epsilon 18x^4 + \epsilon^2 116x^6 + \dots \tag{A 2}$$

and the boundary conditions on these rims read:

$$v_z = - \frac{\partial \psi}{\partial x} = \mp 1, \tag{A 3}$$

$$v_x = \frac{\partial \psi}{\partial z} = 0, \tag{A 4}$$

For convenience, $\psi = 0$ is chosen at $z = 0$, so ψ is odd in z . This equation can be solved assuming

$$\psi = \psi_0 + \epsilon \psi_1 + \dots \tag{A 5}$$

where ψ_0 fulfils the boundary conditions (A 3) and (A 4) and $\partial \psi_1 / \partial x = \partial \psi_1 / \partial z = 0$ on the rim of the particle. The solution is given by:

$$\psi_0 = \frac{1}{2}x \left(3 \left(\frac{z}{b} \right) - \left(\frac{z}{b} \right)^3 \right), \tag{A 6}$$

$$\psi_1 = \frac{3}{20}g(x) \left(\frac{z}{b} \right) \left(1 - \left(\frac{z}{b} \right)^2 \right)^2, \tag{A 7}$$

where $g(x) = 4x(b')^2 - 2bb' - xbb''$ and b', b'' are the first and second derivatives of $b = b(x)$, respectively. The pressure along the line $z = 0$ can be calculated by integrating:

$$\left(\frac{\partial p}{\partial x} \right)_{z=0} = -3b^{-3} \left(x + \epsilon \left(\frac{3}{5}g(x) - \frac{1}{2}f(x) \right) \right), \tag{A 8}$$

where $f(x) = 2x(b')^2 - 2bb' - xbb''$. The zz -component of the total stress tensor (the superfix ^[D] indicates the dimensional form)

$$T_{zz}^{[D]} = -p^{[D]} + 2\eta \frac{\partial v_z^{[D]}}{\partial z^{[D]}}$$

reads in dimensionless form

$$T_{zz} = -p + 2\epsilon \frac{\partial v_z}{\partial z} = -p - 2\epsilon \frac{\partial^2 \Psi}{\partial x \partial z},$$

where also T_{zz} has been scaled on $p_0 = a\eta U/h^2$. The (dimensionless) force per unit length, F , on the particle is calculated by integrating T_{zz} along the line $z = 0$ (swopping the order of integration of the $\partial p / \partial x$ term):

$$\begin{aligned} F(\epsilon) &= 2 \int_0^\infty (T_{zz})_{z=0} dx = 2 \int_0^\infty x \left(\frac{\partial p}{\partial x} \right)_{z=0} dx - 4\epsilon \int_0^\infty \left(\frac{\partial^2 \Psi}{\partial x \partial z} \right)_{z=0} dx \\ &= \int_0^\infty \frac{3x}{b^3(x)} \left(2x + \epsilon \left(\frac{6}{5}g(x) - f(x) \right) \right) dx - 4\epsilon \int_0^\infty \frac{3}{2b^2} (b - xb') dx. \end{aligned} \tag{A 9}$$

This expression can be rewritten as:

$$F(\epsilon) = F_0 + \epsilon(F_1 - F_2),$$

where

$$F_0 = \int_0^\infty \frac{6x^2}{(1 + \frac{1}{2}x^2)^3} dx = \frac{3}{4}\pi\sqrt{2} = 3.3322,$$

$$F_1 = \int_0^\infty \frac{3x}{(1 + \frac{1}{2}x^2)^3} \left(\left(\frac{25}{10}x^3 - \frac{3}{5}x - \frac{6x^5}{(8 + 4x^2)} \right) \right) dx = \frac{207}{80}\pi\sqrt{2} = 11.496,$$

$$F_2 = \int_0^\infty 6 \frac{(1 - \frac{1}{2}x^2)}{(1 + \frac{1}{2}x^2)^2} dx = 0.0,$$

are numerical constants. In our simulations, we have erroneously used a value of $F_1 = 12.829$, which lead to about 1% overestimation of the lubrication force. The lubrication force per unit length in dimensional form, $F^{[D]} = p_0\sqrt{ah}F$, follows from (A 9) as:

$$F^{[D]} = \left(\frac{h}{a}\right)^{-3/2} \eta U F(h/a) = \left(\frac{h}{a}\right)^{-3/2} \eta U \left(F_0 + \frac{h}{a}F_1\right), \quad (\text{A } 10)$$

which expression is correct in first order of ϵ .

REFERENCES

- ACRIVOS, A., BATCHELOR, G. K., HINCH, E. J., KOCH, D. L. & MAURI, R. 1992 Longitudinal shear-induced diffusion of spheres in a dilute suspension. *J. Fluid Mech.* **240**, 651.
- AIDUN, C. K. & LU, Y. 1995 Lattice Boltzmann simulation of solid particles suspended in fluid. *J. Stat. Phys.* **81**, 49.
- BALL, R. C. & MELROSE, J. R. 1995 Lubrication breakdown in hydrodynamic simulations of concentrated colloids. *Adv. Colloid Interface Sci.* **59**, 19.
- BATCHELOR, G. K. & GREEN, J. T. 1972 The hydrodynamic interaction of two small freely-moving spheres in a linear flow field. *J. Fluid Mech.* **56**, 375.
- BEHREND, O. 1995 Solid–fluid boundaries in particle suspension simulations via the lattice Boltzmann method. *Phys. Rev. E* **52**, 1164.
- BHATNAGAR, P., GROSS, E. P. & KROOK, M. K. 1954 *Phys. Rev.* **94**, 511.
- BRADY, J. F. & BOSSIS, G. 1985 The rheology of concentrated suspensions of spheres in simple shear flow by numerical simulation. *J. Fluid Mech.* **155**, 105.
- BRADY, J. F. & MORRIS, J. F. 1997 Microstructure of strongly sheared suspensions and its impact on rheology and diffusion. *J. Fluid Mech.* **348**, 103.
- BREEDVELD, V., VAN DEN ENDE, D., TRIPATHI, A. & ACRIVOS, A. A. 1998 The measurement of the shear-induced particle and fluid tracer diffusivities in concentrated suspensions by a novel method. *J. Fluid Mech.* **375**, 297.
- BREEDVELD, V., VAN DEN ENDE, D., BOSSCHER, M., JONGSCHAAP, R. J. J. & MELLEMA, J. 2001 Measuring shear-induced self-diffusion in a counterrotating geometry. *Phys. Rev. E* **63**, 1(021403).
- CHAPMAN, B. K. & LEIGHTON, D. T. 1991 Dynamic viscous resuspension. *Intl J. Multiphase Flow* **17**, 469.
- DA CUNHA, F. R. & HINCH, E. J. 1996 Shear-induced dispersion in a dilute suspension of rough spheres. *J. Fluid Mech.* **309**, 211.
- DRAZER, G., KOPLIK, J., KHUSID, B. & ACRIVOS, A. 2002 Deterministic and stochastic behaviour of non-Brownian spheres in sheared suspensions. *J. Fluid Mech.* **460**, 307.
- ECKSTEIN, E. C., BAILEY, D. G. & SHAPIRO, A. H. 1977 Self-diffusion of particles in shear flow of a suspension. *J. Fluid Mech.* **79**, 191.

- FENG, J., HU, H. H. & JOSEPH, D. D. 1994a Direct simulation of initial value problems for the motion of solid bodies in a Newtonian fluid. Part 1. Sedimentation. *J. Fluid Mech.* **261**, 95.
- FENG, J., HU, H. H. & JOSEPH, D. D. 1994b Direct simulation of initial value problems for the motion of solid bodies in a Newtonian fluid. Part 2. Couette and Poiseuille flows. *J. Fluid Mech.* **277**, 271.
- FOSS, D. R. & BRADY, J. F. 1999 Self-diffusion in sheared suspensions by dynamic simulation. *J. Fluid Mech.* **401**, 243.
- FRISCH, U., HASSLACHER, B. & POMEAU, Y. 1986 Lattice-gas automata for the Navier–Stokes equation. *Phys. Rev. Lett.* **56**, 1505.
- HAW, M. D., POON, W. C. K. & PUSEY, P. N. 1994 Structure factors from cluster–cluster aggregation simulation at high concentration. *Physica A* **208**, 8.
- HOFFMAN, R. L. 1998 Explanations for the cause of shear thickening in concentrated colloidal suspensions. *J. Rheol.* **42**, 111.
- KRIEGER, I. M. 1972 Rheology of monodisperse lattices. *Adv. Colloid Interface Sci.* **3**, 111.
- KRIEGER, I. M. & DOUGHERTY, T. J. 1959 A mechanism for non-Newtonian flow in suspensions of rigid spheres. *Trans. Soc. Rheol.* **3**, 137.
- LADD, A. J. C. 1994a Numerical simulations of particulate suspensions via a discretized Boltzmann equation. Part 1. Theoretical foundation. *J. Fluid Mech.* **271**, 285.
- LADD, A. J. C. 1994b Numerical simulations of particulate suspensions via a discretized Boltzmann equation. Part 2. Numerical results. *J. Fluid Mech.* **271**, 311.
- LADD, A. J. C. & VERBERG, R. 2001 Lattice-Boltzmann simulations of particle–fluid suspensions. *J. Stat. Phys.* **104**, 1191.
- LYON, M. K. & LEAL, L. G. 1998 An experimental study of the motion of concentrated suspensions in two-dimensional channel flow. Part 1. Monodisperse systems. *J. Fluid Mech.* **363**, 25.
- MARCHIORO, M. & ACRIVOS, A. 2001 Shear-induced particle diffusivities from numerical simulations. *J. Fluid Mech.* **443**, 101.
- NGUYEN, N.-Q. & LADD, A. J. C. 2002 Lubrication corrections for Lattice-Boltzmann simulations of particle suspensions. *Phys. Rev. E* **66**, 1(046708).
- NIRSCHL, H., DWYER, H. A. & DENK, V. 1995 Three-dimensional calculations of the simple shear flow around a single particle between two moving walls. *J. Fluid Mech.* **283**, 273.
- QIAN, Y. H., D’HUMIÈRES, D. & LALLEMAND, P. 1992 Lattice BGK models for the Navier–Stokes equation. *Europhys. Lett.* **17**, 479.
- SHAKIB-MANESH, A., RAISKINMKI, P., KOPONEN, A., KATAJA, M. & TIMONEN, J. 2002 Shear stress in a Couette flow of liquid–particle suspensions. *J. Stat. Phys.* **107**, 67.
- SIEROU, A. & BRADY, J. F. 2001 Accelerated Stokesian dynamics simulations. *J. Fluid Mech.* **448**, 115.
- SIEROU, A. & BRADY, J. F. 2004 Shear-induced self-diffusion in non-colloidal suspensions. *J. Fluid Mech.* **506**, 285.
- TAYLOR, G. I. 1932 The viscosity of a fluid containing small drops of another fluid. *Proc. R. Soc. Lond. A* **138**, 41.
- WANG, Y., MAURI, R. & ACRIVOS, A. 1996 The transverse shear-induced liquid and particle tracer diffusivities of a dilute suspension of spheres undergoing a simple shear flow. *J. Fluid Mech.* **327**, 255.
- YURKOVETSKY, Y. 1998 I. Statistical mechanics of bubbly liquids; II. Behavior of sheared suspensions of non-Brownian particles. Dissertation, Californian Institute of Technology, USA.